Journal of Solid State Chemistry 181 (2008) 2332–2337

Contents lists available at ScienceDirect

Journal of Solid State Chemistry

journal homepage: www.elsevier.com/locate/jssc

Phase transformation and optical properties of Cu-doped ZnS nanorods

Anuja Datta *, Subhendu K. Panda, Subhadra Chaudhuri

Department of Materials Science, Indian Association for the Cultivation of Science, Kolkata 700 032, India

ARTICLE INFO

Article history:
Received 4 February 2008
Received in revised form
12 May 2008
Accepted 26 May 2008
Available online 26 June 2008

Keywords:
Nanorods
Solvothermal
Doping
Phase transformation
UV–vis
Photoluminescence

ABSTRACT

ZnS nanorods doped with 0–15 mol% of Cu have been prepared by simple solvothermal process. With gradual increase in the Cu concentration, phase transformation of the doped ZnS nanorods from wurtzite to cubic was observed. Twins and stacking faults were developed due to atomic rearrangement in the heavily doped ZnS nanorods during phase transformation. UV–vis–NIR absorbance spectroscopy ruled out the presence of any impure Cu–S phase. The doped ZnS nanorods showed luminescence over a wide range from UV to near IR with peaks at 370, 492–498, 565 and 730 nm. The UV region peak is due to the near-band-edge transition, whereas, the green peak can be related to emission from elementary sulfur species on the surfaces of the nanorods. The orange emission at 565 nm may be linked to the recombination of electrons at deep defect levels and the Cu(t_2) states present near the valence band of ZnS. The near IR emission possibly originated from transitions due to deep-level defects.

1. Introduction

One-dimensional semiconductor phosphor nanocrystals have been extensively studied for the last one decade because of their unusual structural, electronic, and optical properties that show interesting applications in advanced optoelectronic systems [1–5]. Doping with optically active luminescent materials manipulate the band structure of the nanocrystals and show intense emissions in a wide range of wavelength depending on the impurity type, concentration and crystal dimensions, and also play key roles in luminescence efficiency and the positions of emission bands, thus influencing their practical applications. Apart from that, crucial structural alterations can also happen due to doping which is important for fundamental understanding of the structure and optical processes in semiconductors [6–8].

ZnS is an important phosphor material because of its wide and direct band gap, which possesses significantly large exciton binding energy (38 meV) compared to the low thermal energy (25 meV at 273 K) that can be utilized for designing efficient room temperature exciton devices [9]. At ambient conditions, pure ZnS crystallizes in two allotropic forms, namely, cubic-ZnS (zinc blende) and hexagonal-ZnS (wurtzite), where wurtzite is the metastable phase at room temperature. Highly desirable physical and chemical properties can be achieved from ZnS nanowires, nanorods, nanobelts, etc. that can be functionalized for applications in diodes, field effect transistors, electro-optic modulators, optical coatings, electroluminescent materials and phosphors in flat panel displays [10–12]. Cu-doped ZnS bulk phosphors are one of the most well-studied luminescent materials and have attracted much attention in context of their technologically suitable fluorescent properties [13–15]. ZnS can host large radii ions of Cu^{2+} and Cu^{+} (atomic radius 0.71 and 0.74 Å, respectively, in four-fold coordination) where Zn-ion can be easily substituted by Cu-ion because Zn is more active in chemical reactions than Cu. Research on ZnS:Cu nanoparticles, including preparation and property characterization [7,16–19], has been carried out. However, studies of the effect of Cu^{2+} concentration on the luminescence of ZnS one-dimensional nanostructures are very limited and remain a subject of great interest.

In this paper, we are reporting the Cu doping induced phase transformation from wurtzite to cubic with an increase in dopant concentration, in solvothermally prepared ZnS nanorods. We also discuss about the possible mechanism of the phase transformation and investigate the photoluminescence (PL) properties from the Cu-doped ZnS nanorods, which is a very novel observation.

2. Experimental

Cu-doped ZnS nanorods were synthesized by a solvothermal technique using ethylenediamine and water as the solvent in a volume ratio of 3:2. Typically, 0.015 mol of Zn-nitrate and Cu-acetate (0–15 mol% of the Zn^{2+} source) were dissolved in the solvent, which was filled up to 80% of the volume of a Teflon container with 110 ml capacity. After stirring for 30 min, 0.045 mol

* Corresponding author. Fax: +91 33 2473 2805.
E-mail address: msad@iacs.res.in (A. Datta).

0022-4596/$ - see front matter © 2008 Elsevier Inc. All rights reserved.
doi:10.1016/j.jssc.2008.05.037

thiourea was added to the container, which was then sealed inside a stainless-steel chamber and inserted in a furnace preheated at 200 °C. The reaction was stopped after 12 h and the chamber was gradually air cooled to room temperature. Cu-doped ZnS nanorods were collected from the Teflon container after repeated washing with distilled water and ethanol. The product was vacuum dried for 6 h and the prepared powder was used for all characterization.

The products were analyzed by X-ray diffractometer (XRD, Seifert 3000P) with Cu $K\alpha$ radiation in the scan range of 20–80°. Microstructures and crystal structures of the nanorods were studied using transmission electron microscopy (TEM) and high-resolution TEM (HRTEM, JEOL 2010). The composition analysis was performed by an Oxford Energy Dispersive X-ray Analyzer (EDAX) attached with the TEM. Absorbance spectra were recorded using a UV–vis–NIR spectrophotometer (Hitachi U-4100) and PL measurements were carried out at room temperature using a fluorescence spectrophotometer (Hitachi, F-2500) with an excitation wavelength of 300 nm.

3. Results and discussion

Ethylenediamine is a well-known chelating agent and has long been used as a very popular template medium for the synthesis of CdE (E = S, Te, Se) one-dimensional nanostructures [20]. However, in case of ZnE (E = S, Se), the thermodynamic and kinetic factors are not suitable to give rise to elongated nanostructures using only ethylenediamine as the solvent. When ethylenediamine is mixed with water, the covalent organic–inorganic hybrid material based on the lamellar $[ZnS]_{\infty}$ units, made up of zinc atom coordinated with three sulfur atoms and one nitrogen atom, stack one after another along the c-axis and give rise to one-dimensional form [21,22]. Due to this reason the samples were prepared by solvothermal process under the mixed solvent.

Fig. 1 shows the XRD patterns of the Cu-doped ZnS nanorods. Results of some intermediate doping percentage have been omitted to avoid clustering. As evident from the figure, undoped and low concentration of Cu^{2+}- (0.1–1 mol%) doped ZnS nanorods show intense and sharp reflections conforming the wurtzite structure of ZnS (JCPDS card no. 36-1450). As the Cu concentration was increased (above 1 mol%), the XRD pattern shows the emergence of an additional peak at $2\theta = 33.4°$, specifically associated with the cubic phase of ZnS (JCPDS card no. 05-0566), indicating that both wurtzite and cubic phases of ZnS co-exist in a single sample. On increasing the dopant concentration to 15 mol%, the peaks of wurtzite ZnS at $2\theta = 26.9°$ and 30.6° corresponding to the (100) and (101) peaks, respectively, became absent and the pattern became similar to the cubic form of ZnS. Considering the fact that wurtzite ZnS is a thermodynamically metastable phase at ambient conditions; the stability and subsequent phase transformation in ZnS nanocrystallites was achieved by adjusting the surface energy through controlled Cu doping. Earlier for ZnS nanocrystals phase transformation was reported to be due to nanosize effect [23]. Later Wang et al. [2] reported phase transformation in ZnS nanobelts, which they interpreted as morphology-tuned. They insisted that some particular morphology enhances the stability of metastable phases by tuning the surface-energy density. In our case, the phase transformation cannot be related to the morphology, because it remains same on varying the dopant concentration. The phase transformation may be facilitated in presence of organic solvent molecules that is able to reduce the difference in free energy of formation between the wurtzite and cubic form of ZnS (10.25 kJ M^{-1} at 298 K and 1 atm) [2,24,25]. The formation of chemical bonds between the surface zinc atoms of ZnS nanocrystals and the $-NH_2$ groups of ethylenediamine molecules alter the surface energy of ZnS nanorods, which may be a reason for the formation of the hexagonal ZnS nanorods [24,25]. When ethanol was used as the solvent, cubic ZnS nanoparticles were obtained and no phase transformation phenomenon was noticed on Cu doping, which gives an indication that surface passivation by ethylenediamine

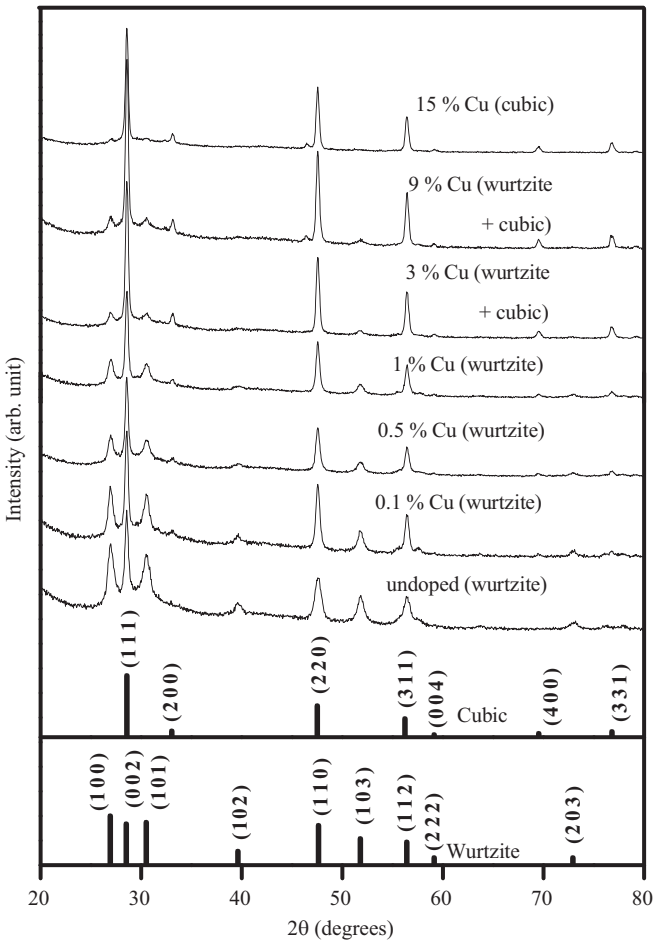

Fig. 1. XRD patterns of the undoped and different percentage of Cu-doped ZnS nanorods with indicating structural phases. Standard bar diagrams for wurtzite and cubic ZnS have been shown at the bottom.

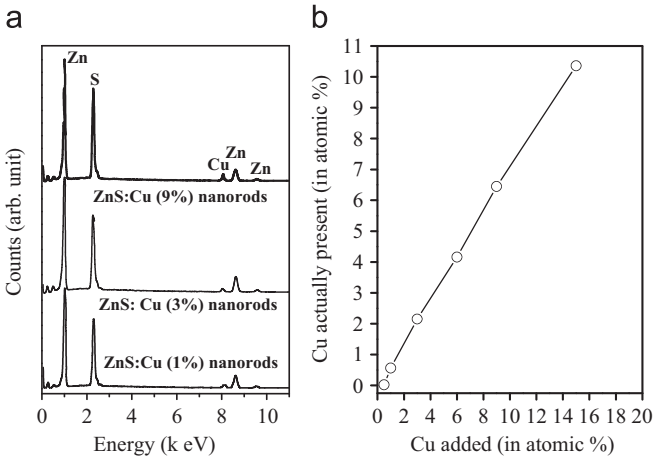

Fig. 2. (a) EDAX spectrum of three different percentages of Cu-doped ZnS nanorods. (b) Graph showing the actual atomic percentage of Cu doped vs. added Cu atomic percentage in different mol% of Cu-doped ZnS nanorods.

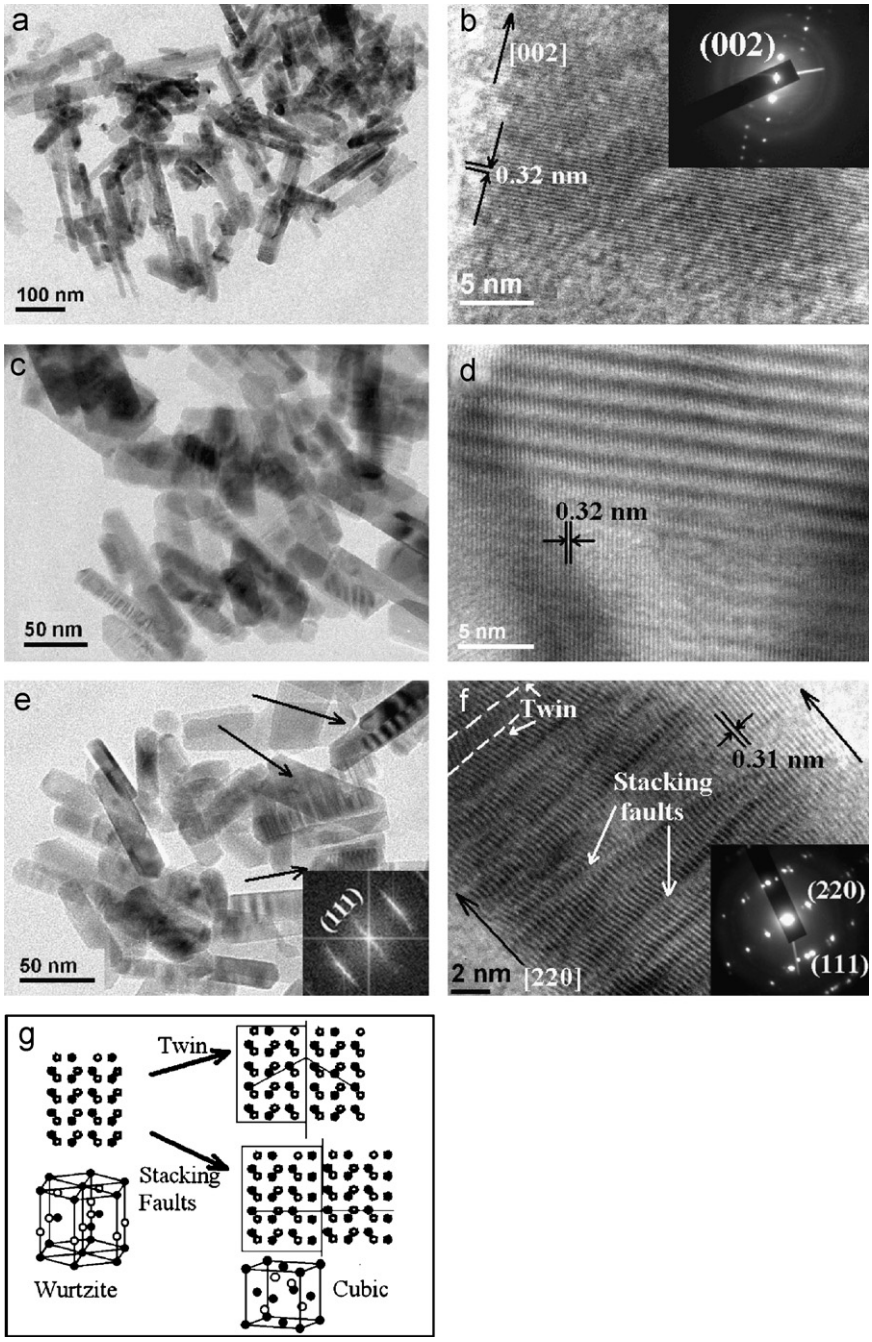

Fig. 3. (a) TEM image and (b) HRTEM image of undoped wurtzite ZnS nanorods with the SAED pattern shown in the inset of (b). The arrow indicates the growth direction of a nanorod. (c) Low-resolution TEM image of 1% Cu-doped wurtzite ZnS nanorods and (d) shows the corresponding HRTEM picture. (e) Image showing the distribution of 15% Cu-doped cubic ZnS nanorods with arrows pointing out the rippled surfaces. Inset shows the FFT indicating cubic structure. (f) HRTEM image of a 15% Cu-doped cubic nanorod with the SAED pattern in the inset. Black arrows indicate the boundaries of the nanorod and white arrows indicate the defects. Schematic diagram for phase transformation process from wurtzite to cubic ZnS has been shown in (g).

molecules is a guiding factor [15]. With substitution of Zn^{2+} ions in the ZnS lattice by Cu ions, a small change in the site symmetry may induce that give a trigger to overcome the required activation energy and instigated the phase transformation from hexagonal to the cubic [25,26].

The composition analysis of the ZnS nanorod samples carried out by EDAX (Fig. 2a), indicated stoichiometric ratio of Zn and S in all the samples. Presence of Cu in the system was also confirmed but it was noted that the percentages of actually doped Cu in the ZnS host are slightly lower than that was added during the reaction. Fig. 2b shows a graph for the percentage of Cu added to the reaction system vs. percentage of Cu actually present in the system.

In order to understand the phase transformation process in this system, we have systematically studied the microstructural properties of the undoped and Cu-doped ZnS nanorods, acquired by TEM. Fig. 3a shows low-resolution TEM image of bunches of undoped nanorods with a nearly uniform diameter of 12–16 nm and length of 150–250 nm. HRTEM image of a single nanorod as shown in Fig. 3b indicates the continuity of the lattice fringes over a long range without any crystal disorder. The observed lattice fringes are separated by a distance of 0.32 nm, corresponding to the (002) plane spacing of wurtzite ZnS. The nanorods were found to grow along the [002] axis. Inset shows the SAED pattern indicating the single crystalline nature of the nanorods with

growth direction along the [002] axis. Fig. 3c is the TEM image of 1 mol% Cu-doped ZnS nanorods. The diameter and the length of the 1 mol% Cu-doped nanorods are nearly the same as that of the undoped ZnS nanorods. HRTEM image (Fig. 3d) shows that the low percentage of Cu-doped ZnS nanorods have incorporated some lattice defects. However, no variation in lattice plane spacing was observed for 1% Cu-doped ZnS nanorods. From TEM image (Fig. 3e), the average diameter and length of the 15 mol% doped ZnS nanorods were measured as 18 and 250 nm, respectively, indicating slight increment in nanorod dimensions. Interestingly, many of the nanorods showed rippled surfaces (shown by arrows). The FFT pattern of the 15 mol% Cu-doped nanorods has been shown in the inset, which is a representative of the cubic structure. Elongation of the spots along the growth axis indicates the presence of defects. The HRTEM image (Fig. 3f) of a 15 mol% Cu-doped nanorod indicated several dislocation and lattice disorders including non-periodic twining and stacking faults along the axial direction of the nanorods. In this case also the lattice spacing was measured to be ~0.31 nm, which well matches with (002) plane of wurtzite and (111) plane of cubic ZnS. Considering our XRD study and close observations of the HRTEM image and FFT pattern, this may be concluded that the lattice fringes represent the cubic structure of ZnS. Inset picture of Fig. 3f shows the SAED pattern, revealing single crystalline nature of the nanorods with the existence of twinning. Moreover, few streaky spots are found in the pattern, which may come from the defects in the lattices. The lattice plane disorders may be introduced during phase transformation to minimize the surface free energy. In wurtzite ZnS, the (0 0 1) plane has the highest surface free energy of 0.91–1.52 J m^{-2} in comparison to the (110) and (100) planes, whereas, in cubic ZnS the (111) plane is the highest energy plane [2,27]. Both the Zn and S atoms in wurtzite and cubic ZnS are four coordinated and thus requires only a minor rearrangement of atoms during phase transformation, where the high energy (111) planes of cubic ZnS grow on the expense of (001) plane of wurtzite ZnS. The rearrangement of three and four stacking cell units of wurtzite ZnS at a time, leads to the development of (111) twinning and stacking faults, respectively in cubic ZnS. Both types of rearrangement phenomena have been well observed in the HRTEM image of 15% Cu-doped ZnS nanorods. The twinning and stacking faults indicate high-energy structural imperfections, for which the phase transformation may be the key energy contributor. There is slight difference in the atomic radius between the Cu ions (0.71 Å) and the Zn^{2+} (0.74 Å), and the migration of Cu ions in ZnS take place by the simultaneous replacement of Zn^{2+}. Fig. 3g shows the basic structure of wurtzite and cubic ZnS going through the atomic rearrangement processes. The development of twining and stacking faults during the rearrangement has also been schematically shown.

To investigate the tailored optical properties of Cu-doped ZnS nanorods, optical absorbance and PL spectroscopy were performed. In order to detect the presence of impure Cu–S phases, which have low band gap values, the optical absorbance spectra were recorded from UV to NIR wavelength region. Absorbance spectra were recorded by ultrasonically dispersing the ZnS nanorods in 2-propanol, which are shown in Fig. 4. Wurtzite phase of ZnS has a bulk band gap of ~3.77 eV and cubic phase shows a band gap value of ~3.72 eV at room temperature [6]. The closeness of the absorption peaks of all the samples to the corresponding bulk ZnS crystals are attributed to the near-band-edge free excitons. Considering the Bohr exciton radius of ZnS to be ~2.5 nm [23], the prepared ZnS nanorods have a weak quantum confinement regime and have not shown marked shift in the absorption bands. Other than the absorbance band of ZnS, no additional band for copper sulfide was detected from the

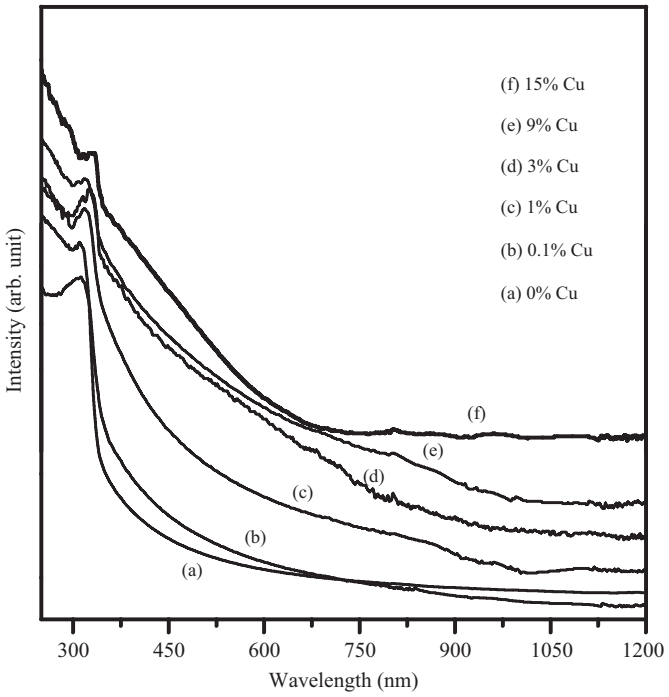

Fig. 4. Optical absorption spectra of the undoped and different percentage of Cu-doped nanorods in UV–NIR range.

spectra extended to longer wavelength, also indicating the phase purity of the doped nanorods.

Fig. 5a depicts the room temperature PL spectra of the undoped and Cu-doped ZnS nanorod samples. Three peaks for the undoped and four peaks for Cu-doped ZnS nanorods were observed from the spectra. For the convenience we divided the spectra into three regions and discussed separately:

(A) Fig. 5b shows the magnified spectra of UV region with a strong and stable emission band at 370 nm for both the undoped and Cu-doped ZnS nanorods. The emission intensity was observed to be maximum for the undoped wurtzite nanorods and it gradually decreased with increasing Cu concentration. Unlike in other reports, where the UV emission from ZnS nanocrystals were related to trap state emission or some other donor-to-acceptor level transitions [7,28], the emission here can be designated as a near-band-edge type because the FWHM of the peak remains nearly unchanged irrespective of doping. For all the samples, the position of this UV band gradually red shifted when excited at different wavelengths, which is possibly due to the distribution of different sized nanorods, where the larger ones absorb and emit at longer wavelengths relative to smaller nanorods [29]. The red shift in the UV band compared to the absorption edge may be explained as due to the splitting of the valence band to two hole states Γ_8 and Γ_7 [30]. The transition from the higher energy Γ_8 state give rise to absorption band and the Γ_7 hole state which is at lower energy can be responsible for the high energy near-band-edge emission. The decrease in the intensity of the UV emission band in Cu-doped nanorods is perhaps due to the dopant complexes acting as nonradiative centers.

(B) Fig. 5c shows the ten times magnified spectra of the emission bands observed in the visible region. In case of undoped ZnS nanorods, only an intense green emission band has been observed at 492 nm, which is stronger than the near-band-edge emission peak. This band can be ascribed to self-activated sulfur defects and/or interstitial lattice defects. In

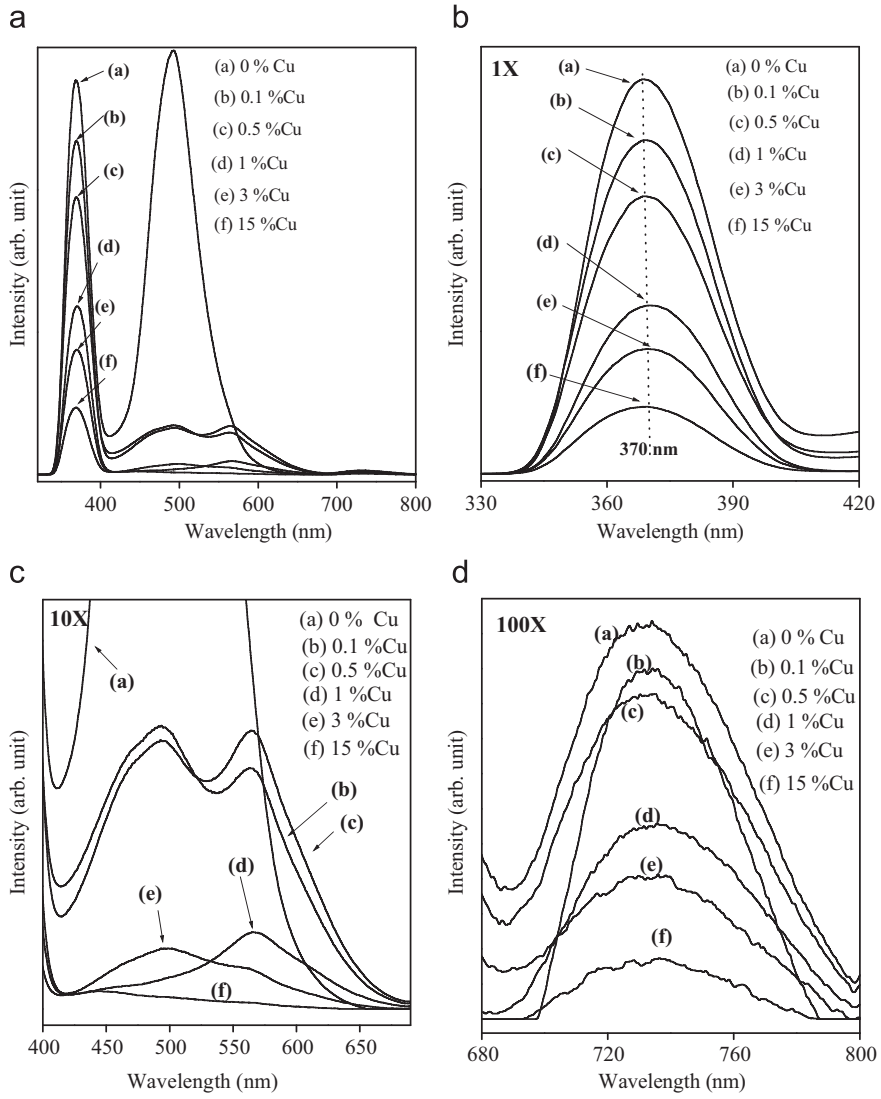

Fig. 5. (a) Room temperature PL spectra of the undoped and Cu-doped ZnS nanorods showing all the emissions within UV–near IR range. Emissions in (b) the UV region, (c) the visible region and (d) the near IR region, have been shown after different magnifications.

undoped and Cu-doped ZnS nanorods which have a larger surface atom ratio and hence higher defect states at the surfaces of the nanorods, the defect related emission is possible as a result of recombination of free charge carriers at defect sites [31–33]. Interestingly, this green emission band becomes negligible for ZnS nanorods synthesized in sulfur deficient condition, thereby suggesting that the green luminescence may have originated from self-activated elementary sulfur species on the surfaces of the undoped and doped ZnS nanorods. It was also observed that under constant UV radiation this emission band suffers an intensity decrement. The prolonged UV radiation is strong enough to initiate surface oxidation process of ZnS nanorods and convert elementary sulfur species on the surfaces to oxides of sulfur and lead to a decreased PL intensity of the green band. The green emission is also very sensitive to the change of the structure. The intensity of the green band decreased substantially upon phase transformation of ZnS nanorods from wurtzite to cubic. Even it was noticed that when doped with Cu in very minute quantity (0.1 mol%), this green emission band red shifts to 498 nm and also quenches significantly. Simultaneously, an orange emission band at ~565 nm appears for the Cu-doped ZnS nanorods. This orange band shows maximum intensity for 0.5 mol% Cu-doped nanorods and experiences a rapid decrease in intensity for higher Cu concentrations. Additionally, the orange emission band broadens for higher dopant concentration. This emission band located at 565 nm for Cu-doped ZnS nanorods is rarely reported so far. Generally, Cu incorporates in ZnS in a Zn^{2+} site as $Cu^{2+}(3d^9)$. Within the tetrahedral crystal field, of the four S^{2-} ligands, the $3d^9$ ground-state splits into higher lying t_2 levels and lower-lying e levels. In bulk ZnS doped with Cu, this kind of low-energy emission comes from a transition between a deep localized donor level like S^{2-} vacancy and the 't_2' level of excited $Cu^{2+}(d^9)$ impurity, yielding Cu^+ [34]. When an electron is excited to the conduction band it is trapped by deep donor levels and an orange luminescence occurs by recombination at the Cu^{2+} impurity. The quenching of the self-activated green emission band in Cu-doped ZnS nanorods suggests a marked reduction in surface defect states as a result of doping, whereas, the decrease in intensity of the orange emission band is perhaps due to the Cu–Cu clustering in the ZnS lattice. With increase in doping concentration, more and more Cu luminescent centers are introduced in the structure and clustering occurred above a certain concentration. The orange emission band red shifts and becomes broad

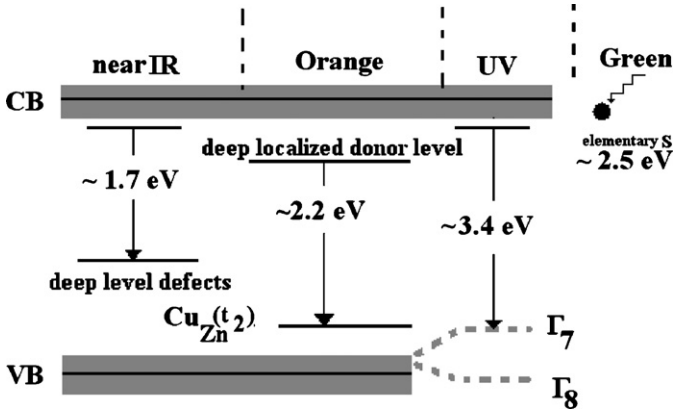

Fig. 6. The schematic energy level diagram of the Cu-doped ZnS nanorods.

because of the release of trapped electrons and holes from the luminescence centers.

(C) Fig. 5d is the near IR emission spectra showing a weak and broad emission band centered at 730 nm for all the samples. In case of the 15 mol% Cu-doped ZnS nanorods only this band appears and no other visible emission are observed to be intense enough, thus showing red luminescence under the UV light. Though the exact reason behind the origin of this red emission is not clear at this moment, the band may possibly originate from numerous defects located at deeper levels of the ZnS band structure. The schematic energy level diagram of the different transitions occurring in Cu-doped ZnS nanorods has been shown in Fig. 6.

4. Conclusions

In conclusion, we have prepared Cu-doped (0.1–15 mol%) ZnS nanorods (diameter 12–18, length 200–250 nm) by solvothermal process. Undoped and up to 1 mol% Cu-doped ZnS nanorods were found to crystallize in wurtzite structure with preferential growth along the [001] direction. With increasing the dopant concentration, the wurtzite ZnS nanorods gradually phase transformed to cubic structure and the growth direction of the nanorods changed along the (111) plane. Phase transformation was also found to induce noticeable defects in the ZnS lattices including twins and stacking faults. A plausible mechanism for phase transformation and origin of the defects has been forwarded. All the samples show luminescence within UV and near IR range. The UV peak is due to band edge emission whereas; the broad peak in the visible region consisting of a green and an orange emission band are contributed by the surface sulfur elements and Cu *d*-states, respectively. The rare and negligible IR emission is possibly from the deep trap states in the ZnS lattice.

Acknowledgments

This work is a dedication to the departed soul of Prof. Subhadra Chaudhuri. A. Datta likes to acknowledge Council of Scientific and Industrial Research, Government of India, for granting fellowship and other research funding during the tenure of this work. The authors also thank Dr. Amitava Patra for his many useful suggestions.

References

[1] Y. Ding, X.D. Wang, Z.L. Wang, Chem. Phys. Lett. 32 (2004) 398.
[2] Z. Wang, L.L. Daemen, Y. Zhao, C.S. Zha, R.T. Downs, X. Wang, Z.L. Wang, R.J. Hemeley, Nat. Mater. 4 (2005) 922.
[3] G. Shen, Y. Bando, D. Golberg, Appl. Phys. Lett. 88 (2006) 123107.
[4] C. Liangf, Y. Shimizu, T. Sasaki, H. Umehara, N. Koshizaki, J. Phys. Chem. B 108 (2004) 9728.
[5] B.Y. Geng, X.W. Liu, Q.B. Du, X.W. Wei, L.D. Zhang, Appl. Phys. Lett. 8 (2006) 163104.
[6] Y.Q. Li, J.A. Zapien, Y.Y. Shan, S.T. Lee, Appl. Phys. Lett. 88 (2006) 013115.
[7] J. Huang, Y. Yang, S. Xue, B. Yang, S. Liu, J. Shen, Appl. Phys. Lett. 70 (1997) 2335.
[8] K. Manzoor, S.R. Vadera, N. Kumar, T.R.N. Kutty, Appl. Phys. Lett. 84 (2004) 284.
[9] S. Velumani, J.A. Ascencio, Appl. Phys. A: Mater. Sci. Process. 72 (2003) 236.
[10] Z.L. Wang, X.Y. Kong, J.M. Zuo, Phys. Rev. Lett. 91 (2003) 185502.
[11] C. Ma, D. Moore, J. Li, Z.L. Wang, Adv. Mater. (Weinheim, Germany) 15 (2003) 228.
[12] M. Bredol, J. Merikhi, J. Mater. Sci. 33 (1998) 471.
[13] A. Ortíz, M. García, A. Sánchez, C. Falcony, J. Electrochem. Soc. 136 (1989) 1232.
[14] S. Shinoya, W.M. Yen, Phosphor Handbook, CRC Press, Washington, DC, 1999.
[15] A. Datta, S. Biswas, S. Kar, S. Chaudhuri, J. Nanosci. Nanotechnol. 7 (2007) 3670.
[16] A.A. Khosravi, M. Kundu, L. Jatwa, S.K. Deshpande, U.A. Bhagwat, M. Sastry, S.K. Kulkarni, Appl. Phys. Lett. 67 (1995) 2702.
[17] S.J. Xu, S.J. Chua, B. Liu, L.M. Gan, C.H. Chew, G.Q. Xu, Appl. Phys. Lett. 73 (1998) 478.
[18] A.A. Bol, J. Ferwerda, J.A. Bergwerff, A. Meijerink, J. Lumin. 99 (2002) 325.
[19] N. Karar, Solid State Commun. 142 (2007) 261.
[20] A. Datta, S. Kar, J. Ghatak, S. Chaudhuri, J. Nanosci. Nanotechnol. 7 (2007) 677.
[21] X. Chen, H. Xu, N. Xu, F. Zhao, W. Lin, G. Lin, Y. Fu, Z. Huang, H. Wang, M. Wu, Inorg. Chem. 42 (2003) 3100.
[22] Z.X. Deng, C. Wang, X.M. Sun, Y.D. Li, Inorg. Chem. 41 (2002) 869.
[23] S.B. Qadri, E.F. Skelton, D. Hsu, A.D. Dinsmore, J. Yang, H.F. Gray, B.R. Ratna, Phys. Rev. B 60 (1999) 9191.
[24] I. Barin, O. Knacke, O. Kubschewski, Thermochemical Properties of Inorganic Substances, Springer, Berlin, 1977.
[25] H. Tong, Y.-J. Zhu, L.-X. Yang, L. Li, L. Zhang, J. Chang, L.-Q. An, S.-W. Wang, J. Phys. Chem. C 111 (2007) 3893.
[26] M. Grus, A.J. Horodecki, A. Jankowska, A. Skowron, Cryst. Res. Technol. 16 (1981) 49.
[27] B. Gilbert, B.H. Frazer, H. Zhang, F. Huang, J.F. Banfield, D. Haskel, J.C. Lang, G. Srajer, G.De. Stasio, Phys. Rev. B 66 (2002) 245205.
[28] H.S. Bhatti, R. Sharma, N.K. Verma, N. Kumar, S.R. Vadera, K. Manzoor, J. Phys. D: Appl. Phys. 39 (2006) 1754.
[29] W. Hoheisel, V.L. Colvin, C.S. Johnson, A.P. Alivisatos, J. Chem. Phys. 101 (1994) 8455.
[30] N. Chestnoy, R. Hull, L.E. Brus, J. Chem. Phys. 85 (1986) 2237.
[31] W.G. Becker, A.J. Bard, J. Phys. Chem. 87 (1983) 4888.
[32] A.A. Bol, A. Meijerink, Phys. Rev. B 58 (1998) R15997.
[33] D. Denzler, M. Olschewski, K. Sattler, J. Appl. Phys. 84 (1998) 2841.
[34] S. Shionoya, K. Urabe, T. Koda, K. Era, H. Fujiwara, J. Phys. Chem. Solids 27 (1966) 865.